JOURNAL OF INFORMATION SCIENCE AND ENGINEERING 32, 677-702 (2016)

Fast Defogging and Restoration Assessment Approach to Road Scene Images*

FAN GUO[1,2], HUI PENG[1,2,3] AND JIN TANG[1]
[1]*School of Information Science and Engineering*
Central South University
Hunan, 410083 P.R. China
[2]*Collaborative Innovation Center of Resource-Conserving and Environment-Friendly Society and Ecological Civilization*
Hunan, 410083 P.R. China
E-mail: huipeng@csu.edu.cn

Single image defogging has received increased attention recently. However, most existing methods are generic restoration methods which may cause partial over-enhancing to the image at a short distance. This certainly makes these defogging methods may be not suitable for road images. In this paper, we propose a new image defogging algorithm that divides the original foggy image into three regions and different enhancement processes are performed for the different region. As the results, the far-away region image that is most concerned by a car driver can be moderately enhanced, and over-enhancement of the bottom region image can be also limited effectively. To effectively measure the defogging effects of various algorithms, the assessment methods based on image feature and visibility distance are proposed for road scene image. The comparative study and quantitative evaluation show that the proposed method can obtain very good defogging image with relatively fast speed.

Keywords: road scene, image defogging, region segmentation, defogging effect assessment, image feature, visibility distance

1. INTRODUCTION

Under adverse weather conditions, the contrast of an image that is grabbed by an in-vehicle camera in the visible light range may be drastically degraded. This makes current in-vehicle applications relying on such sensors very sensitive to weather conditions. An in-vehicle vision system should have excellent image defogging capability [1].

Visibility restoration algorithms generally face three challenges. The first one is to enhance contrast from a single image. Due to the physics of fog, visibility restoration requires the estimation of both the sky intensity and the scene transmission map. This implies that one has to estimate two unknown parameters from a single image. Such a problem is an ill-posed problem. The second challenge is how to obtain a balanced and global enhancement property. For road scene images, the contrast on the road part of the

Received November 30, 2014; revised February 4 & April 1, 2015; accepted May 25, 2015.
Communicated by Chung-Lin Huang.
[3] Corresponding author: Hui Peng.
* This work was supported by the National Natural Science Foundation of China (71271215, 71221061, 91220301, 61502537), the Collaborative Innovation Center of Resource-conserving and Environment-friendly Society and Ecological Civilization, the China Postdoctoral Science Foundation (No. 2014M552154), the Hunan Postdoctoral Scientific Program (No. 2014RS4026), and the Postdoctoral Science Foundation of Central South University (No. 126648), and the International Science & Technology Cooperation Program of China (2011DFA10440).

restored result is often too much enhanced using some existing methods, since the most methods are not to develop to road images, and they also have difficulty in processing a large uniform region, such as the road surface. The third challenge involves measuring the effectiveness of different visibility restoration algorithms. Subjective evaluation, as a main defogging effect assessment method at present, is easily affected by observer's subjective feeling, which may make the evaluation results unreliable.

Because of the importance of the defogging algorithm, much work has been done in the literature. Unfortunately, they are difficult to use for a moving vehicle. For example, some algorithms used the images that are taken at different times [2], or used the images with different polarizing filters [3]. Recently, the fog removal of a single image has made significant progress. Tan [4] restored image contrasts by maximizing the contrasts of the direct transmission. However, the method may produce halos near depth discontinuities. Fattal [5] estimated the transmission in hazy scenes, relying on the assumption that the transmission and the surface shading are locally uncorrelated. Although the algorithm can produce impressive results, 5-7 minutes is needed to process an image with a size of 600×400 using double processors of Pentium 4 and 1 GB memory. He *et al.* [6] removed fog based on the dark channel prior, which is a statistic variable of haze-free outdoor images. For getting a better result, soft matting was used for the transmission estimation. Combined with the atmospheric scattering model, a good restored image can be obtained by this approach. However, He's method is computationally expensive due to the use of matting procedure. Thus, its improvement such as Wei's method [7] was proposed, which does not require computationally expensive processing for achieving reliable restoration results. The algorithm obtained the atmospheric light, and greatly improved the speed and accuracy of atmospheric scattering function that was solved by using gray-scale opening operation and fast joint bilateral filtering techniques. Tarel *et al.* [8] used a fast median filter to infer the atmospheric veil, and further estimated the transmission map. However, the method is unable to remove the fog between small objects, and the color of the scene objects is unnatural for some situations. Besides, all of the above methods are generic restoration methods which are not designed to cope with road images.

This paper presents two main approaches. First, we propose a novel defogging algorithm to automatically restore the contrast of the road scene image that is captured by an on-vehicle camera. The foggy image acquisition system is shown in Fig. 1. The novelty of the proposed method is in dealing with defogging separately at three different regions based on their distance to the car, so that the far-away region image that is most concerned by driver is moderately enhanced, and the over-enhancement of the bottom region image is properly constrained. The essence of image defogging is contrast enhancement, but the defogging is different from generic contrast enhancement, since it needs to estimate the depth information of each pixel to determine the enhancement coefficient. The proposed defogging method combines the depth prior with the contrast transformation of the original image by using the region segmentation. Thus, better defogging effect may be obtained by the proposed method for road images. On the other hand, so far, there is lack of methodology to assess the performance of defogging algorithm. Subjective evaluation, as the main approach to assessing the algorithms at present, is easily affected by observer's subjective feelings, which makes the evaluation results unreliable. Therefore, in this paper we propose an assessment approach that uses image feature and visibility distance as the quantitative measurement indexes, so the defogging effect can be effectively measured for road scene images.

(a) (b) (c)

Fig. 1. Foggy image acquisition system; (a) The vehicle used for collecting data; (b) Placement of the camera on the vehicle; (c) Placement of the computer within the vehicle.

The rest of the paper is organized as follows. In Section 2, we present the atmospheric scattering model and the camera model that are used for image defogging and restoration assessment. In Section 3, we propose a new image defogging algorithm. For measuring the defogging effects of various image defogging algorithms, two defogging effect assessment methods especially for road scene image are introduced in Section 4. The experimental results are reported in Section 5. In Section 6, some applications of the proposed image defogging algorithm are presented. Finally, we give some conclusions in Section 7.

2. BACKGROUND

Assume that for an object of intrinsic luminance L_0, its apparent luminance L in presence of fog of extinction coefficient k is modeled by Koschmieder's law [9] as follows

$$L = L_0 e^{-kd} + L_s(1 - e^{-kd}), \tag{1}$$

where d is the distance of the object, and L_s is the sky intensity. Eq. (1) is known as the atmospheric scattering model. The model indicates that the luminance of the object that is seen through fog is attenuated in e^{-kd} (Beer-Lamber law). Eq. (1) may be rewritten as:

$$L - L_s = (L_0 - L_s)e^{-kd}. \tag{2}$$

Based on this equation, Duntley developed a contrast-attenuation law [9], that is, a nearby object exhibiting contrast C_0 with the background will be perceived at distance d with following contrast [10]:

$$C = [(L_0 - L_s) / L_s]e^{-kd} = C_0 e^{-kd}. \tag{3}$$

This expression is on the basis of the definition of a standard dimension that is called "meteorological visibility distance". According to International Commission on Illumination (CIE), the meteorological visibility distance is defined as the greatest distance at which a black object of a suitable dimension can be seen in the sky on the horizon, with the threshold contrast set 5% [11], that is C/C_0=0.05. Thus, this definition yields the following expression:

$$d_{\max} = -\frac{\ln(0.05)}{k}. \tag{4}$$

For camera response, we first let f denote the camera response function, which models the mapping from scene luminance to image intensity by imaging system, including optic as well as electronic parts [12]. As can be seen in Fig. 2, the intensity I of a pixel is the result of f applied to the sum of the sky intensity A and the direct transmission T:

$$I = f(L) = f(T + A). \tag{5}$$

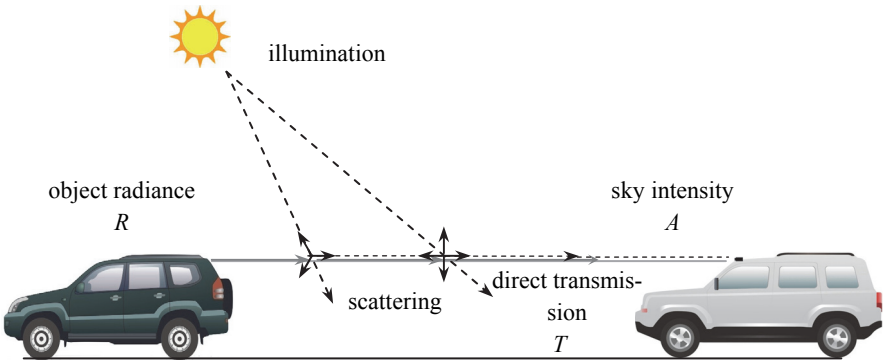

Fig. 2. Atmospheric scattering model. Fog luminance is due to the scattering of light. Light coming from the sun and scattered by atmospheric particles towards the camera is the sky intensity A. It increases with the distance. The light emanating from the object R is attenuated by scattering along the line of sight. Direct transmission T of the scene radiance R decreases with distance.

Suppose that the conversion process between incident energy on the charge-coupled device (CCD) sensor and the intensity in the image is linear, this is a general case for short exposure times, because it prevents the CCD array from being saturated. Furthermore, short exposure times are used on in-vehicle cameras to reduce the motion blur. This assumption can thus be considered as valid and then (5) becomes:

$$\begin{aligned} I &= f(T) + f(A) = f(L_0 e^{-kd}) + f(L_s(1 - e^{-kd})) \\ &= f(L_0)e^{-kd} + f(L_s)(1 - e^{-kd}) \\ &= Re^{-kd} + A_s(1 - e^{-kd}). \end{aligned} \tag{6}$$

For image defogging, I is the input foggy image, R is the restored image. e^{-kd} is the so-called transmission map, which is denoted as t that expresses the relative portion of light, and manages to survive the entire path between the observer and a surface point in the scene, A_s is the background sky intensity. Thus, for a foggy image at pixel (x, y), Eq. (6) can be written as:

$$I(x, y) = R(x, y)t(x, y) + A_s(1 - t(x, y)). \tag{7}$$

According to the camera model established by Hautiere *et al.* [10], we have the following representation. As illustrated in Fig. 3, the position of a pixel is given by its (u, v) coordinates in the image plane. The coordinates of the optical center projection in the image are designated by (u_0, v_0). Let H denote the mounting height of the camera, θ the angle between the optical axis of the camera and the horizontal, and v_h is the vertical position of the horizontal line in the image. The intrinsic parameters of the camera are its local length f_l, and the horizontal size t_{pu} and vertical size t_{pv} of a pixel. From the above three parameters, we can obtain $\alpha_u = f_l / t_{pu}$ and $\alpha_v = f_l / t_{pv}$, and typically we have: $\alpha \approx \alpha_v = \alpha$. Suppose that the road is flat, which makes it possible to associate a distance d with the vertical position of each pixel in the image coordinate system (u, v) which is denoted by v and it is also the row number of each pixel. Therefore, the distance d can be written as:

$$d = \frac{\lambda}{v - v_h}, \text{ where } \lambda = \frac{H\alpha}{\cos\theta}. \tag{8}$$

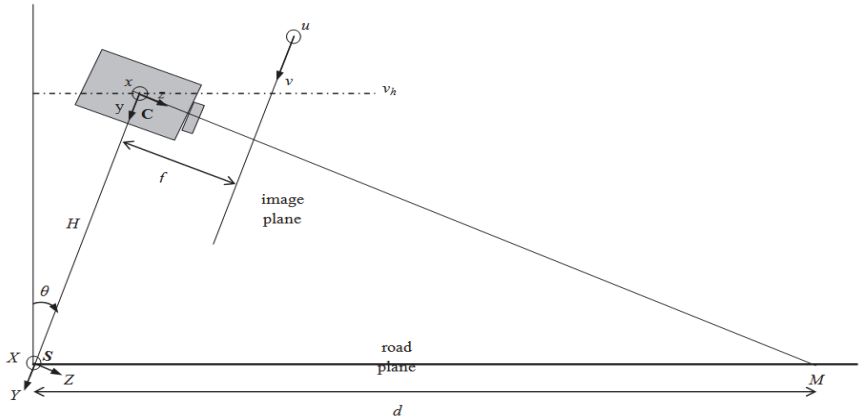

Fig. 3. Modeling of the camera within its environment. It is located at a height of H in the (S, X, Y, Z) coordinate system relative to the scene. Its intrinsic parameters are its focal length f and pixel size t. θ is the angle between the optical axis of the camera and the horizontal. Within the image coordinate system, (u, v) designates the position of a pixel, (u_0, v_0) is the position of the optical center C and V_h is the vertical position of the horizontal line.

Here, introducing $\lambda = H\alpha / \cos\theta$ in Eq. (8) is to make Eq. (8) appear simpler for display purpose. The value of parameter λ can be obtained in two ways. The one is computing λ through camera parameters (*e.g.* H, α and θ), as we mentioned above. The other is to estimate λ through marked targets. To perform the estimation, the actual distance d_1–d_2 between two points and their coordinates v_1 and v_2 in the input image should be first obtained. Then, the parameter λ can be expressed as the following Eq. (9). More details about Eqs. (8) and (9) are given in Appendix A.

$$\lambda = \frac{d_1 - d_2}{\left(\frac{1}{v_1 - v_h} - \frac{1}{v_2 - v_h}\right)} \tag{9}$$

3. PROPOSED DEFOGGING ALGORITHM

A new image defogging algorithm is proposed in this section. The proposed algorithm may achieve very good enhancement results for road scene image by giving a road plane assumption into the atmospheric scattering model. Fig. 4 depicts the flowchart of the image defogging algorithm. It can be seen that there are three key steps for restoring road scene image: sky intensity estimation, transmission map estimation and scene radiance recovery. Thanks to the enhancement coefficient map, the far-away region image that is most concerned by driver is moderately enhanced and the over-enhancement of the bottom region image may be properly constrained.

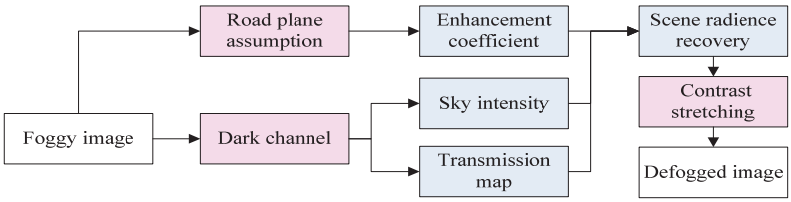

Fig. 4. Algorithm flowchart for image defogging. The intermediate steps are shown as red blocks and the key steps are shown as blue blocks.

3.1 Sky Intensity and Transmission Map Estimation

Estimating sky intensity A_s should be the first step to remove fog from the input foggy image. Different from He's method [6] that obtains A_s in RGB color space, our process is based on the key observation, that is, the effect of sky intensity can be shown more intuitively in hue-saturation value (HSV) color space than in RGB color space. Thus, it is sufficient to limit the analysis on the saturation component S for estimating sky intensity. Specifically, this process can be written as:

$$S(x,y) = 1 - \min_{c\in\{r,g,b\}} I^c(x,y) / \max_{c\in\{r,g,b\}} I^c(x,y), \tag{10}$$

where $I^c(x, y)$ is the original foggy image at pixel (x, y), c represents the three color channels of the RGB space, and S is the saturation component of the input image. Let $D(\cdot)$ denote the operation of dark channel calculation, thus the dark channel of an image I is denoted as $D(I)$. According to the dark channel prior [6] proposed by He *et al.*, the process is given by the following operation:

$$D(I) = \min_{(k,l)\in\Omega(x,y)} (\min_{c\in\{r,g,b\}} I^c(k,l)). \tag{11}$$

Similarly, $D(R)$ represents calculating the dark channel of the restored image R. Thus, $D(R)$ can be written as:

$$D(R) = \min_{(x',y')\in\Omega(x,y)} (\min_{c\in\{r,g,b\}} R^c(x',y')). \tag{12}$$

In Eq. (11), $\Omega(x, y)$ is a local $N \times N$ patch centered at (x, y). Therefore, saturation component S can be related to the dark channel by substituting (10) into (11), it yields

$$D(I) = \min_{(k,l)\in\Omega(x,y)} (\max_{c\in\{r,g,b\}} I^c(k,l)(1-S(k,l))). \tag{13}$$

From Eq. (13), we can deduce that the addition of a high amount of the sky intensity increases the value of the saturation component of HSV. Besides, for the regions of images with dense fog, $\max I^c$ in (13) tends to be 1. Thus, the dark channel can be approximately expressed using the saturation component S which is denoted by $D(S)$ as follows:

$$D(I) \approx D(S) = \min_{(k,l)\in\Omega(x,y)} (1-S(k,l)). \tag{14}$$

Therefore, the sky intensity A_s can be estimated as a color vector of a pixel (x, y) in image I with maximum intensity at locations corresponding to a small subset of the highest intensity pixels $\{x_{D(S)}, y_{D(S)}\}$ of the dark channel $D(S)$, which usually is located in the sky regions in the image. That is $A_s = \max I(x,y), \quad (x,y) \in \{x_{D(s)}, y_{D(s)}\}$. For the restored image R in Eq. (7), its dark channel $D(R) \to 0$ according to the dark channel prior proposed by He *et al.* [6]. This property is useful in eliminating the unknown scene radiance from Eq. (7) by first dividing the equation by A_s and then applying minimum operator to its both sides:

$$\min_{c\in\{R,G,B\}} \left\{ \min_{(x',y')\in\Omega(x,y)} \left(\frac{I^c(x',y')}{A_s} \right) \right\} = t(x,y) \min_{c\in\{R,G,B\}} \left\{ \min_{(x',y')\in\Omega(x,y)} \left(\frac{R^c(x',y')}{A_s} \right) + \left(1-t(x,y)\right) \right\}. \tag{15}$$

From Eqs. (11) and (12), the Eq. (15) can be rewritten as:

$$\frac{D(I)}{A_s} = \frac{D(R)}{A_s} t(x,y) + (1-t(x,y)). \tag{16}$$

Ideally, the minimum intensity in a patch of the ideal fog-free image should be zero according to the dark channel prior proposed by He *et al.*, that is $D(R) \to 0$. A constant parameter ω is also introduced to make the image look more natural. Therefore, the transmission map t can be computed by:

$$t(x,y) = 1 - \frac{\omega D(I)}{A_s}. \tag{17}$$

where ω is the mean value of the dark channel of $D(S)$, and it is used to account for a small amount of fog that can be seen at high distances even on clear day.

3.2 Scene Radiance Recovery

Scene radiance recovery is the most important step for improving the visibility of road scene image. However, most existing defogging algorithms perform the same visibility restoration process for the whole image region, which are not suitable for the pro-

cess of road image with large and uniform region such as road. For road scene image, it is very rare to observe fog at a short distance in practice, thus the contrast in the bottom part of the resulting image, which is often a road part, may be over-enhanced if the far away objects are properly enhanced. To overcome the problem, the enhanced strength of the image in bottom region should be constrained to prevent the over-enhancement of the part near road, and we must make sure that the far-away region image that is most concerned by driver can be enhanced moderately.

To achieve this goal, the image region segmentation is performed to divide the image into three parts: the sky, the far-away objects, and the plane near road, and different enhancement processes are performed for the different region image to prevent over-enhancement of the bottom part of the image. According to Eq. (4), extinction coefficient k is related to the distance $d_{\max}$ by $k = -\ln(0.05)/d_{\max}$. Assume that the road is a plane until a certain distance, and the camera calibration is known with respect to the road, thus λ and v_h are known. Therefore, we define the estimation process of the segmentation image as:

$$G(x,y) = 1 - e^{-kd} = 1 - e^{\frac{\ln(0.05)\lambda}{d_{\max}(v - v_h)}}. \tag{18}$$

In Eq. (18), the parameter λ depends on intrinsic and extrinsic parameters of the camera, such as H, α and θ according to Eq. (8), v represents each line of the image, v_h is the vertical position of the horizon line image, and $d_{\max}$ is a estimated threshold value.

In practice, if the distance between the scene points and the observer is lower than the value $d_{\max}$, it is very rare that fog is observed. The value of $d_{\max}$ is application-based. We set it to 140 for all the 600×400 images reported in this paper. For an image with a size of $M \times N$, the value of $d_{\max}$ should be estimated according to the practical conditions, and the value of $d_{\max}$ can be set within the range of meteorological visibility distance, that is the $d_{\max}$ value that used in Eq. (18) can be less than or equal to the meteorological visibility distance in practical calculations. Besides, $\ln(0.05)$, $\lambda = (H\alpha)/\cos\theta$, $d_{\max}$ and v_h in Eq. (18) are all constant. v in Eq. (18) is the vertical position of each pixel in the image coordinate system and it is also the row number of each pixel. For an input image with a size of $M \times N$, its v can be also regarded as an image, whose pixel value can be written as $(u, v) = v$ ($u \in \{1, ..., N\}$, $v \in \{1, ..., M\}$). Therefore, the computing result of Eq. (18) can be presented as an image. An illustrative example of estimated segmentation image is shown in Fig. 5 (c). One can clearly see that the segmentation image $G(x, y)$ denotes the part with emphasis on far-away objects by relatively higher image intensity, and other parts are represented by relatively lower intensity. Thus, we can define three kinds of segmentation regions according to the intensity value: top region that is called "sky" region, middle region that is called "far-away scene" region, and the bottom region that is called "road surface" region. The three segmentation regions are determined for each image pixel using the estimated meteorological visibility distance. Next, the actual distance of each pixel in the input road image is computed according to the camera model, and different enhancement coefficients are assigned for each image region. Since the fog density is positive correlation to the actual distance, and the larger value of the fog density should correspond to the larger value of the enhancement coefficient, we can thus determine the enhancement coefficient of each image pixel by its actual distance.

Therefore, the three segmentation regions are obtained by the meteorological visibility distance, and different enhancement processes for different region are performed by using the enhancement coefficient map.

By combining the segmentation image with the atmospheric scattering model, the segmentation image prevents the bottom region image to be over-enhanced. With the segmentation image G, we can obtain the restored image R using Eq. (7). Since the term $R(x, y)t(x, y)$ will be very close to zero when the transmission $t(x, y)$ is close to zero, so the transmission $t(x, y)$ should be restricted to a lower bound t_0 to preserve a small amount of fog in very dense foggy regions. A typical value of t_0 is 0.1. The R is thus recovered by:

$$R(x, y) = \frac{I(x, y) - A_s}{\max(t(x, y), t_0)} G(x, y) + A_s. \tag{19}$$

From Eq. (19), we can see that different enhancement coefficients are given to the predefined three image regions by virtue of the segmentation image G. Therefore, the three regions "sky", "far-away scene" and "road surface" of the input foggy image have different enhancement effects to ensure that the far-away region that is most concerned by driver can be moderately enhanced, and the enhancement of the bottom region image can be properly constrained. In Fig. 5, since we already know the original foggy image $I(x, y)$ [see Fig. 5 (a)], the estimated transmission map $t(x, y)$ [see Fig. 5 (b)], the segmentation image $G(x, y)$ [see Fig. 5 (c)], and the sky intensity A_s, we can take these values into Eq. (19) to obtain the restored image $R(x, y)$.

Finally, an adaptive contrast stretch process is performed on the restored image R to ensure that the contrast of the far-away region image is stretched and the contrast of the image at bottom region is also improved without over-enhancement. Thus, our final defogging image R_f can be obtained as:

$$R_f(x, y) = \left(\frac{R(x, y) - V_{low}}{V_{high} - V_{low}} \right) \times 255 \tag{20}$$

where V_{low} and V_{high} are the minimum and maximum threshold values for the adaptive contrast stretch process. All the color channels of the restored image R will be stretched using the same threshold values to preserve the correct color ratio. The two values can be determined as follows

$$\begin{aligned} V_{low} &= \arg_{R_i}(L(R_i) > Th, L(R_i) > L(R_{i-1})), \\ V_{high} &= \arg_{R_i}(L(R_i) \geq 1 - Th, L(R_i) > L(R_{i-1})). \end{aligned} \tag{21}$$

In Eq. (21), $L(R_i)$ denotes the cumulative histogram of the restored image $R(x, y)$. Specifically, let n_i be the number of occurrences of gray level i. The probability of an occurrence of a pixel of level i in the image R is

$$R_i = P_R(i) = \frac{n_i}{n} \quad 1 \leq i < 256, \tag{22}$$

where n is the total number of pixels in the image, and R_i is the image's histogram for pixel value i, which is normalized to [0,1]. Thus, the cumulative distribution function corresponding to the image R can be defined as:

$$L(R_i) = \sum_{j=0}^{i} P_R(j). \tag{23}$$

Besides, the parameter Th in Eq. (21) is the threshold parameter used to prevent outliers from scaling, and we fix it to 0.02 in our experiment. Thus, the final fog removal result for road scene image can be obtained as shown in Fig. 5 (d).

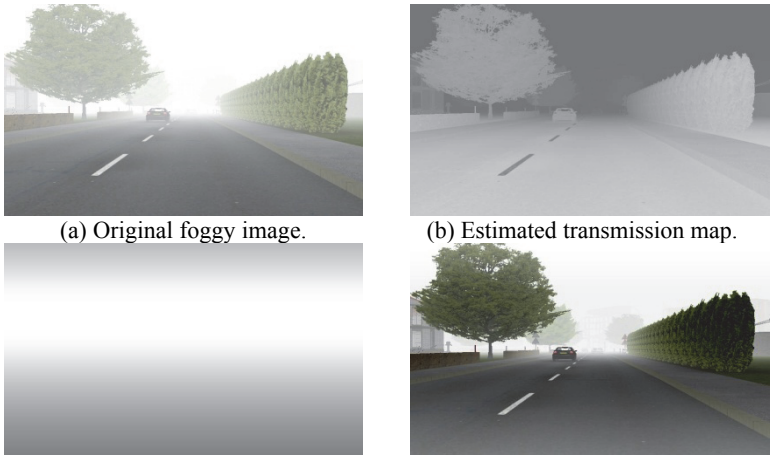

(a) Original foggy image. (b) Estimated transmission map.

(c) Enhancement region segmentation image G. (d) Our result.

Fig. 5. Steps of the proposed defogging algorithm for road scene image.

4. DEFOGGING EFFECT ASSESSMENT

Since there is lack of methodology to assess the performance of defogging algorithm and the existing assessment methods have some limitations, two new methods for assessing the defogging algorithm are proposed in this section. The one is using image feature to assess the defogging algorithm. The method regards the point clusters that are formed by the image RGB histogram as a color ellipsoid in geometry. Based on the observation, the assessment method associates the image defogging effect with the centroid and the volume of the color ellipsoid. The other one is to compute the visibility distance before and after image restoration, since the visibility distance is the most direct and effective way to evaluate the restoration capacity of image defogging algorithms.

4.1 Defogging Algorithm Assessment Based on Image Feature

The assessment way is based on the following observation on a large quantity of natural scene images, *i.e.*, the subsets of the color clusters that are formed by the RGB histogram in natural images are ellipsoidal in shape, and the image features represented

by the centroid and the volume of the color ellipsoids are tied to the image defogging effect. If the centroid is closer to the origin of the RGB coordinate and the volume is larger, it demonstrates that the defogging effect of the fog removal method is better, otherwise, the defogging effect is worse. As can be seen in Fig. 6, for the patches in the original foggy image, the ellipsoid is smaller in size, it is positioned farther away from RGB origin. While for the same position patches in the fog removal result, the ellipsoid is larger in size, it is positioned closer to the RGB cube origin. That's because the process of using ellipsoid properties to remove fog is actually trying to make the defogging image darker on average and make its color more colorful at the same time. Therefore, we can deduce that the defogging effect can be effectively evaluated by the properties of the color ellipsoid, which the centroid of the ellipsoid is related to the image luminance and the volume of the ellipsoid is related to the color colorfulness. Based on the analysis, we propose adopting image luminance and color colorfulness as the defogging effect indexes. The luminance index LI can be defined as:

$$\mathrm{LI} = \mathrm{mean}(\mathrm{IM}), \tag{24}$$

$$\mathrm{IM} = \frac{\sum_{c\in\{\mathrm{R,G,B}\}} \underset{(x',y')\in\Omega(x,y)}{\mathrm{med}} I^c(x',y')}{3}, \tag{25}$$

where I is the input image, 'med' represents the image median operator, and 'mean' operation is performed on the matrix IM, and the operation includes two steps: transforming the matrix IM into one-dimensional column vector, and obtaining the mean value of the column vector. Using the luminance index LI, the centroid of the color ellipsoid can be effectively measured. The larger LI value demonstrates the ellipsoid positioned farther away from RGB origin, which corresponds to a relatively worse defogging effect. Otherwise, the smaller LI value demonstrates the ellipsoid positioned closer to RGB origin, and a relatively better defogging effect is obtained.

Another feature used for defogging effect assessment is the image color colorfulness, and the volume of the ellipsoid is related to the color colorfulness, as shown in Fig. 6. As can be seen in the figure, the larger of the ellipsoid size, the more colorful of the image will be. That's because the color ellipsoid is formed by the point clusters of RGB histogram. Apparently, the more spread of the distribution of the point clusters in RGB coordinates, the more colorful of the input image is. In order to measure the image colorfulness, the Color Colorfulness Index (CCI) [13, 14] which describes the vividness degree of image color is adopted in the paper. Yendrikhovskij [15] introduces a model for optimal color image reproduction of natural images which are based on the assumption that the color colorfulness is one of the most important factors for assessing image quality of natural images. Thus, Hasler [14] gives a very nice and efficient way of computing the colorfulness. He assumes that the image is coded in the sRGB color space and gives the colorfulness metric CCI. Therefore, the relation between the two concepts is that the size of color distribution of pixels in a sample patch reflects the image color colorfulness, and the color colorfulness can be measured by the index CCI. The lager CCI value demonstrates the ellipsoid is larger in size, which corresponds to a relatively better defogging effect. Otherwise the defogging effect is worse.

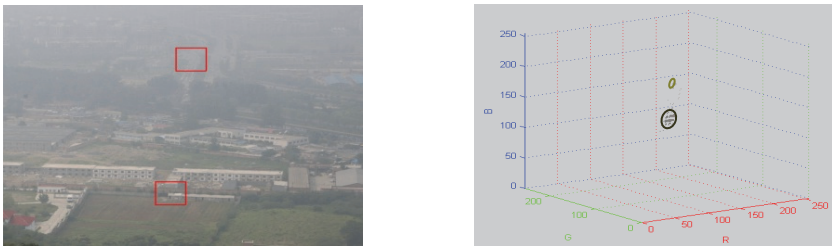

(a) Original foggy image with two sample windows. (b) RGB histogram of each sample set for (a).

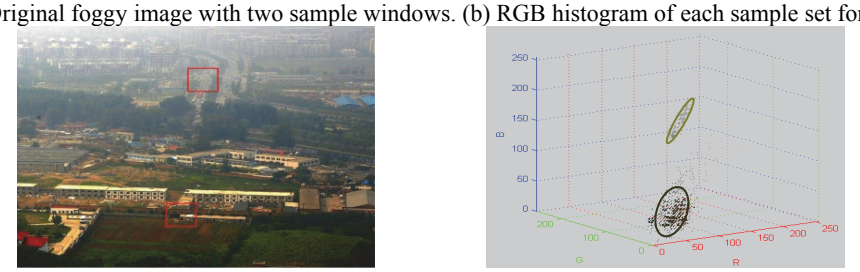

(c) Fog removal image with two sample windows. (d) RGB histogram of each sample set for (c).

Fig. 6. Color ellipsoids in the natural scenes before and after defogging.

4.2 Defogging Algorithm Assessment Based on Visibility Distance

The concept of visibility distance is proposed based on the Koschemieder's law [9]. According to the mathematical properties of the law, the existence of an inflection point can be detected on the image. Once we have the vertical positions of the inflection point and the horizontal line, we can obtain the image line representative of the visibility distance. Then, the image line representative in the image coordinate system can be transformed into real visibility distance by virtue of Eq. (8). Specifically, using visibility distance to assess image defogging effect mainly consists in four key steps: camera parameter estimation, target region detection, bandwidth measurement and visibility distance computation.

The camera parameters used for image defogging are the vertical position of the horizon line v_h and the camera parameter λ. Specifically, to estimate the two parameters, we first mark the targets in white on the road, and the distances between the first five targets and the camera from near to far are 5, 7, 9, 11, 13 meters [see Fig. 7 (b)]. Then, we manually choose four line segments. From the bottom of the image, the sequences are [5th target, 4th target], [4th target, 3rd target], [3rd target, 2nd target], [2nd target, 1st target], as shown in Fig. 7 (c). The marker sequences are corresponding to d = [13 11; 11 9; 9 7; 7 5]. With any pair of the markers, the parameter λ can be obtained using Eq. (9), where parameter v_h is inferred as follows, and more details are given in Appendix A.

$$v_h = \frac{y_1 d_1 - y_2 d_2}{(d_1 - d_2)} \tag{26}$$

In Eq. (26), y_1 and y_2 are the vertical ordinate of the marked 5th and 4th targets, respectively. d_1 and d_2 are the corresponding actual distance values, so d_1 = 13 and d_2 = 11. Similarly, the other three pairs of v_h and λ can also be obtained following the same steps.

Thus, the average of the four pairs of the two parameters is the final parameter value. In our experiment, the parameter values calculated for Fig. 7 (a) are $v_h = 879$ and $\lambda = 3633$. Since different cameras and different cars have different values of v_1 and v_2, so the values of v_h and λ are different accordingly. Therefore, we can deduce that the two parameters v_h and λ are camera dependent and car dependent. Besides, as we mentioned before, the parameter can be also expressed as $\lambda = H\alpha/\cos\theta$. Since different cameras and cars have different parameter settings, thus the same conclusions that the two parameters are camera and car dependent can be drawn.

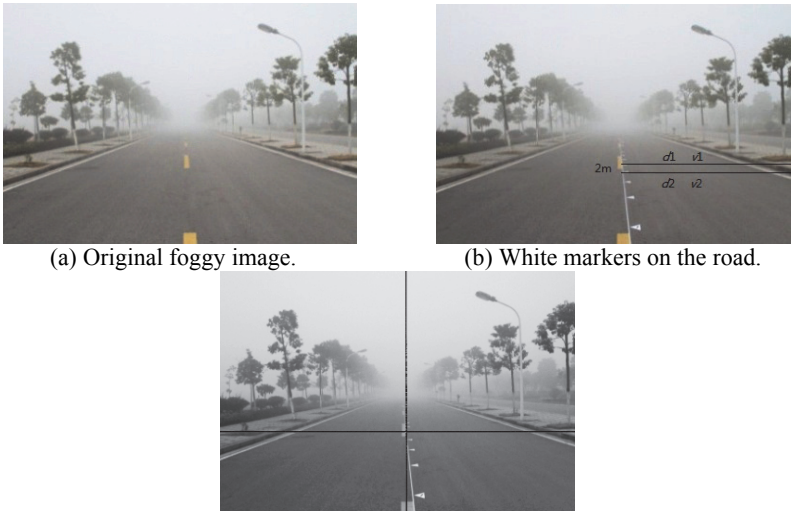

(a) Original foggy image. (b) White markers on the road.

(c) The manually chosen line-segments.

Fig. 7. Steps of camera parameter estimation.

Once the two camera parameters v_h and λ are estimated, the image contours are extracted to highlight the major contrast breaks constituting the road edges, vehicles ahead or crossing, trees, *etc.* This edge extraction step is performed by the canny detection. The two parameters of canny detection t_L and t_H are respectively set to be 0.06 and 0.25 to exclude noise during contour detection and thereby avoid obtaining an interruption at level of the horizon line. An example of canny edge detection is shown in Fig. 8 (a).

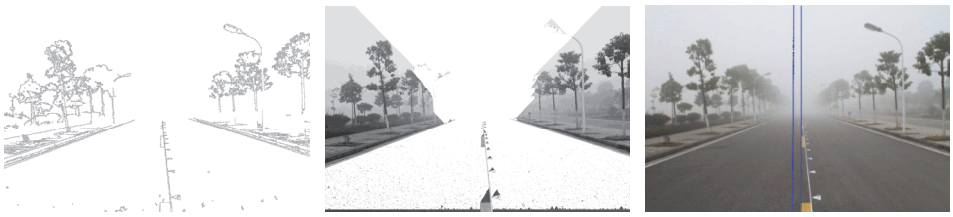

(a) (b) (c)

Fig. 8. Target region detection and bandwidth measurement; (a) Canny edge detection result; (b) Region growing result (the target region is painted in white); (c) Measurement bandwidth computation (blue lines).

The next step is to perform a region growing algorithm to extract target region. The objective of the algorithm is to identify a region within the image that displays minimal gradient variation. Here, we use the region growing method which is widely used in image segmentation to identify the proper region. The method is classified as a pixel-based image segmentation method, since it involves the selection of initial seed points. Specifically, this approach to segmentation examines neighboring pixels of initial seed points and determines whether the pixel neighbors should be added to the region. The process is iterated on in the same manner as general data clustering algorithms. In our application, the initial seed points of region expansion for an image with a size of M×N are chosen as the pixels of a line from the image height M-20. The gray level of these pixels lies close to the median value of the gray levels of the initial line to ensure that the segmented region displays minimal line-to-line gradient variation when crossed from bottom to top. In our experiment, if the difference between the pixel intensity and the median value is less than 10, the pixel is selected as a new seed for region expansion. Fig. 8 (b) gives the region growing result for the original image shown in Fig. 7 (a). Then, the luminance variation over a vertical bandwidth with a maximum width is measured. The measurement bandwidth for Fig. 7 (a) is shown on the blue lines in Fig. 8 (c). Once the measurement bandwidth is obtained, the median luminance of each bandwidth line L can be computed. Then, a smoothing of L is performed such that this function is decreasing in order to avoid the detection of too many local inflection points. Fig. 9 (a) shows the curve representative of the median luminance of the bandwidth. The derivative of L then gets calculated and smoothed afterward, as shown in Fig. 9 (b). The local minimum positions are the position of the inflection point v_i, which minimizes the squared error between the issued model and the measured curve. The vertical position of the horizontal line v_h can be obtained using Eq. (26), and the camera parameter λ can be obtained using Eq. (9). Thus, according to the Eq. (8), the visibility distance V can be computed by:

$$V = \frac{\lambda}{v_v - v_h}, \tag{27}$$

where $v_v = \frac{2v_i + v_h}{3}$. (28)

Note that v_v denotes the image line representative of the visibility distance in the form of pixel unit, we can then use Eq. (27) to transform it (unit: pixel) into real distance (unit: meter). The visibility distance V estimated from Fig. 9 (c) is 86.5 meters.

Besides, for image defogging effect assessment, what we care most is the relatively increased value of the visibility distance. Since the same visibility estimation process is performed on the fog removal results of various defogging algorithms, thus the increased distance value can be regarded as a reliable index for algorithm evaluation even the two parameter values are different for different cameras and cars.

5. EXPERIMENTAL RESULTS

To demonstrate the effectiveness of the proposed method, we used synthetic images and real captured images of road scenes in the experiments. Results on a variety of road scene images show that the proposed method is fast enough to be used in real-time applications.

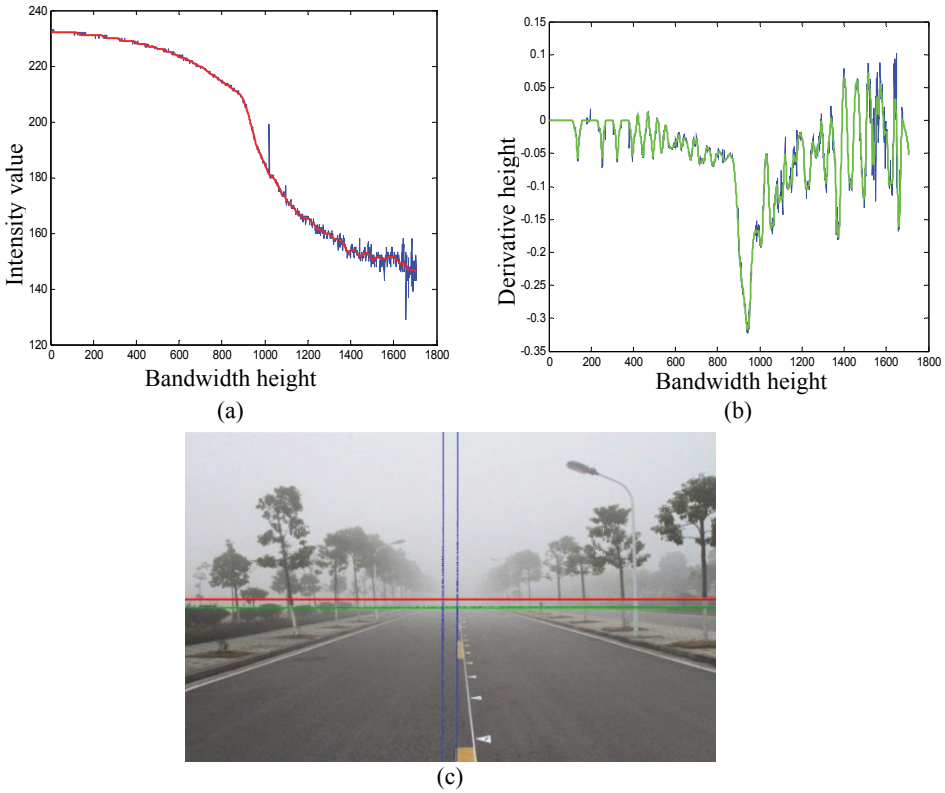

Fig. 9. Curve representative of the measurement of vertical luminance variation in the foggy image; (a) The curve of the median luminance of the bandwidth (blue–without smoothing; red–with smoothing); (b) The derivative of the curve (blue–without smoothing; green–with smoothing); (c) Visibility distance measurement. The measurement bandwidth is shown in vertical blue lines. The horizontal green line represents an estimation of visibility distance v_v, and the horizontal red line represents the vertical position of the horizontal line v_h.

5.1 Qualitative Comparison

To evaluate the performance of various defogging algorithms, we first use synthetic images due to the difficulty of acquiring a scene with and without fog. The synthetic images with uniform fog from the database FRIDA [16] are used here. The representative image defogging algorithms used for comparison are: He's algorithm [6] and Tarel's algorithm [8], since He's algorithm is recognized as one of the most effective ways to remove fog, and Tarel's algorithm is regarded as one of the fastest defogging algorithms at present. The sample results obtained using the two state of the art methods and the proposed algorithm on the FRIDA databases are shown in Fig. 10. Notice the increase of the contrast for the farther objects where there are the buildings and trees that are barely visible in foggy image in Fig. 10. The farther objects appear more clearly in our restored images, compared with the restored results obtained by He's method and Tarel's method. The results on other testing images of the FRIDA database also confirmed the observation.

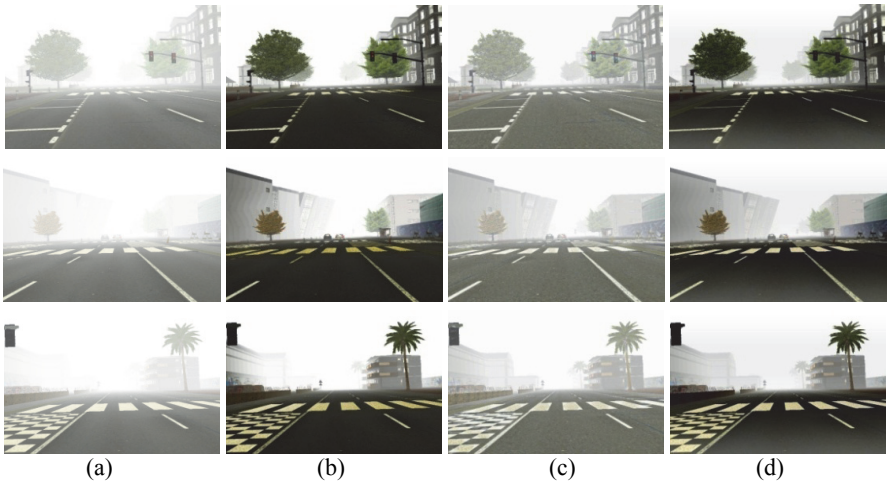

(a) (b) (c) (d)

Fig. 10. Comparison of defogging results for synthetic foggy images; (a) Original foggy image; (b) He's restored results; (c) Tarel's restored results; (d) Our restored results.

Besides, the proposed algorithm also works well for a wide variety of real captured foggy images. Fig. 11 shows the comparison of our results and Wei's method [7]. One can clearly see that the over-enhancement occurs at short distance in the Wei's results, while both the near and far part of our results have been enhanced properly.

Fig. 11. Comparison of defogging results. First row: Original foggy image. Second row: Wei's restored results. Third row: Our restored results.

Fig. 12 shows some examples of the defogging effects obtained using He's method, Taral's method and the proposed algorithm. It can be seen that the image contrast and detail are greatly improved by using the three image defogging algorithms. However, the near road surface in He's results is over-enhancement, which makes the color of whole image seem unnatural. The defogging results of Tarel's method seem not visually pleas-

ing and many halo artifacts also occurs in the results. Using the proposed method, the far-away region that is most cared by driver is moderately enhanced, and the over-enhancement of the bottom region image is effectively avoided, as shown in Fig. 12 (d).

(a) (b) (c) (d)

Fig. 12. Comparison of defogging results for real captured foggy images; (a) Original foggy image; (b) He's restored results; (c) Tarel's restored results; (d) Our restored results.

5.2 Quantitative Evaluation

In this section, we use the assessment methods presented in Section 4 to quantitatively assess defogging methods. Table 1 shows the statistical results for Fig. 11. From Table 1, we can see that the proposed method generally has lager value of CCI, but sometimes have larger value of LI compared to the other results. This indicates that each defogging algorithm has to make a trade-off between contrast enhancement and color fidelity. Compared with Wei's method, the proposed method, as a whole, can get a better trade-off between LI and CCI, so this demonstrates that similar or better quality results may be obtained by using the proposed method.

Table 1. Comparison with Wei's method using the two indicators based on image feature.

Indicator	LI	CCI	LI	CCI
Method	Fig. 11 (Column 1)		Fig. 11 (Column 2)	
Wei [7]	113.2688	0.2052	104.0219	0.2547
Proposed	101.0678	0.4120	115.9054	0.5480
Method	Fig. 11 (Column 3)		Fig. 11 (Column 4)	
Wei [7]	99.9092	0.3254	100.7098	0.3884
Proposed	93.9008	0.5778	109.2031	0.5075

Table 2 shows the statistical results for Figs. 10 and 12 using the assessment method based on image feature. From Table 2, one can clearly see that compared to others, our algorithm generally gives the smallest LI value. For the color colorfulness index CCI, the

CCI value of the proposed method is generally much larger than Tarel's results and slightly smaller than He's statistical results for the six test images. That is because He's defogging results are sometimes over-enhanced, which makes the image appear more colorful. Thus, we can deduce that our method has better overall quality compared with other methods. This confirms our observation in Figs. 10 and 12, and the effectiveness of the proposed LI index is also verified.

Table 2. Comparison with the state of art defogging algorithms using the two indicators based on image feature.

Indicator	LI	CCI	LI	CCI
Method	Fig. 10 (Row 1)		Fig. 10 (Row 2)	
He [6]	117.6	0.6736	132.7	0.6285
Tarel [8]	171.4	0.2123	180.4	0.1947
Proposed	115.4	0.6938	130.1	0.6773
Method	Fig. 10 (Row 3)		Fig. 12 (Row 1)	
He [6]	144.2	0.6244	151.0	2.4229
Tarel [8]	186.2	0.1977	141.5	2.1734
Proposed	143.3	0.6426	145.5	2.4014
Method	Fig. 12 (Row 2)		Fig. 12 (Row 3)	
He [6]	148.9	1.5890	170.7	2.6796
Tarel [8]	137.5	1.1723	169.2	2.1783
Proposed	118.8	1.4074	144.4	2.5299

The two assessment indexes proposed in this paper are also tested on more sample natural color images (150 test images), which consist of foggy image from internet database and real scene captured by Canon S80 with different scene, weather and fog density. Fig. 13 (a) shows the statistical result of the LI for 150 images, and Fig. 13 (b) shows the CCI result for these test images. The horizontal axes are the assessment index values, and the vertical axes are the image number index. From Fig. 13 (a), it is seen that the LI of the proposed method is generally smaller than that of He's method and Tarels' method. The smaller the value of LI, the better the defogging effect will be. Thus, the conclusion that the proposed method has better defogging effect can be drawn. In Fig. 13 (b), it is clear that the CCI of Tarel's and He's defogged images are distributed between [0, 2.5] and [0.5, 2.5], respectively, and the CCI of our defogged images is clustered between 0 and 3.5. The higher the value of CCI, the better the defogging effect will be. Thus, we deduced that the CCI value of the proposed method is overall greater than that of other methods, and thus our defogging effect is better for the image test database. This is also consistent with the assessment results of the LI and human visual perception.

Another straight-forward way to evaluate the defogging effect of various fog removal algorithms is to estimate the visibility distance of their restored results. To this end, the visibility distance is computed for some typical defogging algorithms, such as Histogram equalization (HE), Retinex, He [6], Tarel [8] and the proposed algorithm. Fig. 14 shows the restored results of these methods, and their corresponding visibility distance obtained by using the computation process presented in Subsection 4.2 are shown in Table 3. From Table 3, one can see that the visibility distance obtained by our proposed method is much larger than that gotten from the other methods. Experiments on other road scene images can also confirm the conclusion.

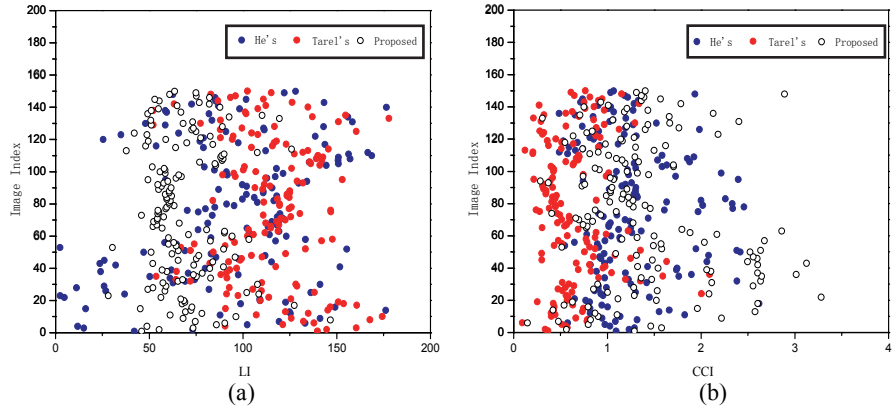

(a) (b)

Fig. 13. Index statistical results for test images; (a) LI; (b) CCI.

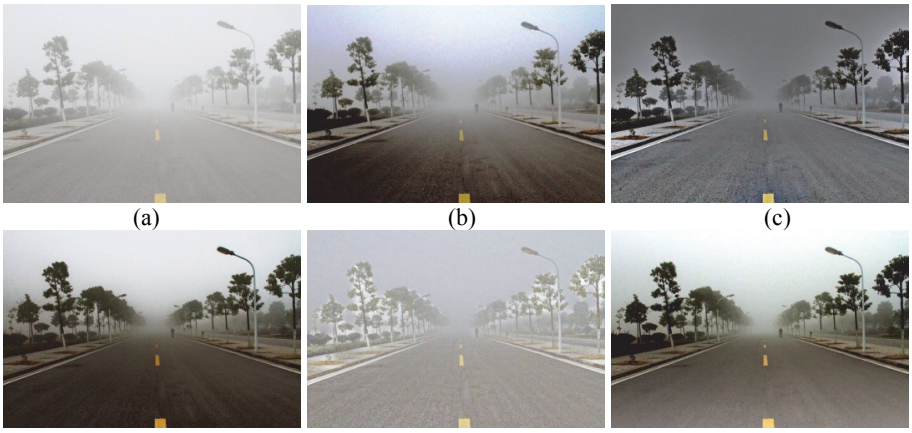

(a) (b) (c)

(d) (e) (f)

Fig. 14. Comparison of defogging results for real captured foggy images; (a) Original foggy image; (b) Histogram equalization result; (c) Retinex algorithm result; (d) He's restored result; (e) Tarel's restored result; (f) Our restored result.

Table 3. Computation results of visibility distance (increased distance value).

Method	Nothing	HE	Retinex	He	Tarel	Proposed
Visibility (meter)	98.2	177.5 (79.3)	182.0 (83.8)	190.3 (92.1)	107.5 (9.3)	201.8 (103.6)

5.3 Computational Time

The computational time is considered by testing the state of art image defogging methods. In our experiments, we performed the algorithms by executing Matlab R2012a on a PC with Core (TM) i5-2400 CPU, 3.10GHz, 4.00GB Memory. For He's method, its computation complexity is relatively high since the matting Laplacian matrix L in the method is so huge, so that for an image of size $s_x \times s_y$, the size of L is $s_x s_y \times s_x s_y$, then 20 seconds are needed to process a 600-by-400 pixels image. The computational time of

Tarel's method is smaller than that of He's method. It takes about 4 seconds to process an image of size 600×400. The proposed method has much faster speed, and only 0.017 second is needed to obtain the restored image with the size of 600×400. That is because the computation complexity of our method is a linear function of the number of input image pixels. Therefore, our method is fast enough to be used in real-time applications.

6. APPLICATIONS

Some applications of the proposed image defogging approach, such as road marking features extraction and road signs detection, are presented in this section, which provides a way to estimate the visibility restoration in a very simple manner.

6.1 Road Marking Features Extraction

Road-marking detection is a fundamental task to develop a camera-based driving assistance system, which aims at avoiding road departure. Road-marking feature extraction is the low-level processing of the road-marking detection. Here, we use the gray histogram-based method proposed by Shan *et al.* [17] to extract road marking features. Two distinctive features of the road markings are considered here: (i) the intensity value of road markings is higher than other road surface and (ii) the road markings have fixed width. Therefore, the regions with higher intensity have more possibility to belong to road marking, and the ratio of the marking width and image width should be in certain range. Thus, for each row of input image, the road marking candidates can be obtained using gray histogram. Then, removing redundant pixels from the candidate areas using the morphological operation, and the road marking features can be effectively extracted. We applied this algorithm to the image given in Fig. 15 (a) and the restored versions of this image using different defogging algorithms are given in Figs. 15 (b)-(d) with the same settings of the algorithm parameters. One can clearly see that for all the defogged results, there is an improvement of the detection range of the road markings, especially the road markings in the distance. However, there are more non-marking pixels that are mistaken as the road marking features using He's method and Tarel's method compared with the result using our method, due to the over-enhancement and the introduced artifacts.

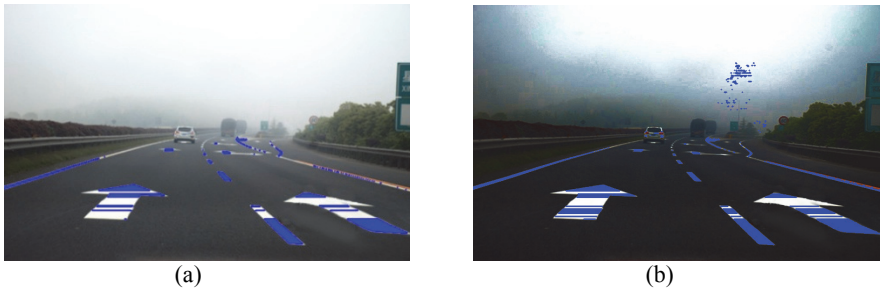

(a) (b)

Fig. 15. Example of road-marking feature extraction; (a) Road-marking extraction in the original image; (b) Road-marking extraction in He's restored image; (c) Road-marking extraction in Tarel's restored image; (d) Road-marking feature extraction in our restored image.

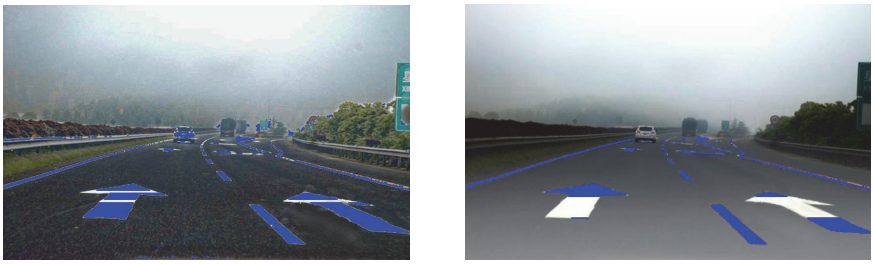

(c) (d)

Fig. 15. (Cont'd) Example of road-marking feature extraction; (a) Road-marking extraction in the original image; (b) Road-marking extraction in He's restored image; (c) Road-marking extraction in Tarel's restored image; (d) Road-marking feature extraction in our restored image.

6.2 Road Marking Features Extraction

The proposed defogging method can also improve the detection of road signs. In China, road signs are designed in the standard geometrical shapes such as circle, octagon, triangle, rectangle, and square, and the distinctive colors are red, blue, yellow, *etc.* The messages of road signs are represented by the specific color and shape. Thus, most algorithms relying on the color and shape detectors, such as method proposed in [18], could benefit from contrast improvement in the images. The sign detection method [18] first changes the RGB color space of the input image to separate each distinctive color of road signs from the surrounding environment with only one threshold value, and then extracts the clockwise boundary of region shape as the shape signatures for detecting road signs. Fig. 16 shows the detection of a square sign using the original foggy image and the restored images obtained using different defogging algorithms.

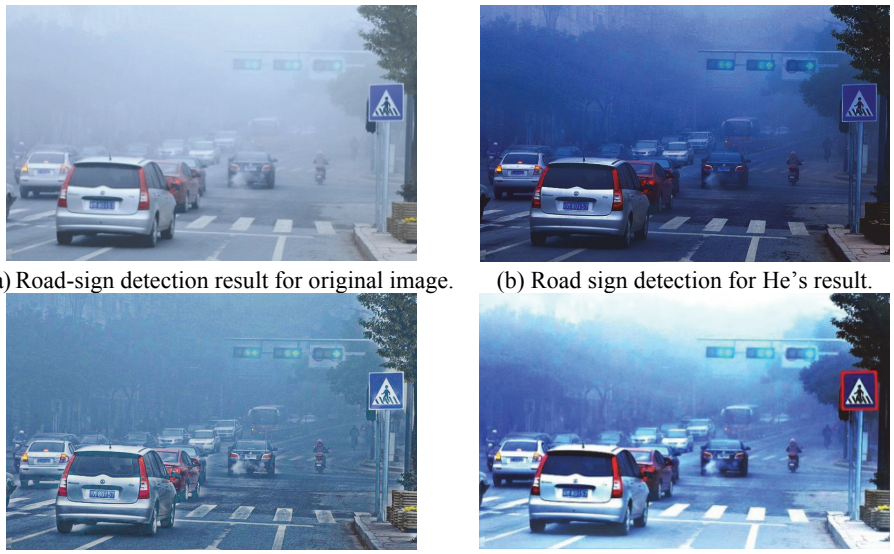

(a) Road-sign detection result for original image. (b) Road sign detection for He's result.

(c) Road-sign detection for Tarel's result. (d) Road-sign detection for our result.

Fig. 16. Example of road-sign detection.

It can be seen from Fig. 16 that the sign is found using the proposed defogging method, whereas it is not found using the original image and other defogged results. The parameters of the detection method are the same in all the cases. The reason for the failure of the result using He's method is that the color of the whole image appears too dark due to the over-enhancement. While for Tarel's result, the road sign is not obvious in the restored image due to the unpleasing defogging effect. All these factors cause the color clue invalid for the sign detection method. Compared to these defogging algorithms, the proposed method may greatly improve the image contrast and preserve a natural color at the same time. Thus, the road sign can be successfully found, as shown in Fig. 16 (d).

7. CONCLUSIONS

In this paper, an image defogging method was proposed for removing fog from road scene image. By properly assigning different enhancement coefficients for each segmentation region, the proposed method could perform different enhancement processes for different region image. Thus, the far-away region image that is most concerned by a driver could be moderately enhanced and the enhancement of the bottom region image could be properly constrained. To quantitatively assess different defogging algorithms, two ways to evaluate the image defogging effect were also introduced. The comparative experiments and quantitative evaluations showed that the proposed method could provide better results for road scene images compared with other representative algorithms.

However, the proposed image defogging method and the assessment methods used for measurement of defogging effect also have some drawbacks. First, the dividing approach to the three regions are based on our daily-life experience, which may make the proposed defogging method somewhat sensitive to the near objects that may accidentally appear in the far-away region of the segmentation image. Besides, the visibility distance computation requires only road and sky existed in the scene, which may also limit its applications in some situations. We hope that all these shortcomings can be solved in the future work.

APPENDIX A: Details about Eq. (8), Eq. (9) and Eq. (26)

Based on the hypothesis of a flat road, it is possible to associate a distance with each line of the image. Using the distance computation model shown in Fig. 3, Eqs. (8), (9) and (26) can be derived as follows.

According to the pinhole model for camera, a point with three-dimensional coordinates (x, y, z) within camera reference system is projected onto the image plane in accordance with the following expression

$$\frac{(u-u_0)t_{pu}}{f_l}=\frac{x}{z}, \tag{A·1}$$

$$\frac{(v-v_0)t_{pv}}{f_l}=\frac{y}{z}, \tag{A·2}$$

where f_l is the local length of the camera, t_{pu} and t_{pv} are the horizontal size and vertical size of a pixel. Within the image coordinate system, (u, v) designates the position of a pixel, and (u_0, v_0) is the position of the optical center. Let $\alpha_u = f_l / t_u$ and $\alpha_v = f_l / t_v$ ($\alpha_u \approx \alpha_v = \alpha$), we have

$$\begin{cases} u = u_0 + \alpha \dfrac{x}{z} \\ v = v_0 + \alpha \dfrac{y}{z} \end{cases}. \tag{A·3}$$

According to Fig. 3, the horizontal line passing through the optical center makes an angle θ with the z-axis of the camera. Within the image plane, the horizon line can therefore be written as

$$v_h = v_0 - \alpha \mathrm{tg}\theta. \tag{A·4}$$

Substituting $v = v_0 + \alpha \dfrac{y}{z}$ into (A·4), we can obtain the following expression

$$\frac{v - v_h}{\alpha} = \frac{y}{z} + \mathrm{tg}\theta. \tag{A·5}$$

Being positioned within the (S, X, Y, Z) real-world coordinate system corresponding to the scene, Eq. (A·5) then becomes

$$\frac{v - v_h}{\alpha} = \frac{Y + H}{Z} + \mathrm{tg}\theta. \tag{A·5}$$

A point M located on the road at a distance d from the origin S get parameterized as

$$\begin{bmatrix} X \\ Y \\ Z \end{bmatrix} = \begin{bmatrix} X \\ -d\sin\theta \\ d\cos\theta \end{bmatrix}. \tag{A·6}$$

Substituting $Y = -d\sin\theta$ and $Z = d\mathrm{cod}\theta$ into Eq. (A·5), we have

$$\frac{v - v_h}{\alpha} = \frac{-d\sin\theta + H}{d\cos\theta} + \mathrm{tg}\theta = \frac{H}{d\cos\theta}. \tag{A·7}$$

Let $\lambda = \dfrac{H\alpha}{\cos\theta}$, the distance d can then be expressed by

$$d = \frac{\lambda}{v - v_h}. \tag{A·8}$$

If we know the actual distance d_1–d_2 between two points and their coordinates v_1 and v_2 in the image, we then have

$$d_1 - d_2 = \frac{\lambda}{v_1 - v_h} - \frac{\lambda}{v_2 - v_h}. \quad \text{(A·9)}$$

Therefore, the parameter λ can ultimately be expressed by

$$\lambda = \frac{d_1 - d_2}{(\frac{1}{v_1 - v_h} - \frac{1}{v_2 - v_h})}. \quad \text{(A·10)}$$

Suppose that y_1 and y_2 are the vertical coordinates of the marked 5th and 4th targets in Fig. 6(b), respectively. Thus, $y_1 = v_1$ and $y_2 = v_2$. d_1 and d_2 are the corresponding actual distance values of these targets. By virtue of Eq. (A·8), we are able to obtain the following:

$$\frac{d_1}{d_2} = \frac{\lambda / (v_1 - v_h)}{\lambda / (v_2 - v_h)}. \quad \text{(A·10)}$$

It can be deduced that

$$v_h = \frac{v_1 d_1 - v_2 d_2}{d_1 - d_2} = \frac{y_1 d_1 - y_2 d_2}{d_1 - d_2}. \quad \text{(A·11)}$$

REFERENCES

1. N. Hautiere, J. P. Tarel, and D. Aubert, "Mitigation of visibility loss for advanced camera-based driver assistance," *IEEE Transactions on Intelligent Transportation Systems*, Vol. 11, 2010, pp. 474-484.
2. S. G. Narasimhan and S. K. Nayar, "Contrast restoration of weather degraded images," *IEEE Transactions in Pattern Analysis and Machine Intelligence*, Vol. 25, 2003, pp. 713-724.
3. Y. Schechner, S. Naraimhan, and S. Nayar, "Polarization-based vision through haze," *Applied Optics*, Vol. 42, 2003, pp. 511-525.
4. R. T. Tan, "Visibility in bad weather from a single image," in *Proceedings of IEEE Conference on Computer Vision and Pattern Recognition*, 2008, pp. 1-8.
5. R. Fattal, "Single image dehazing," *ACM Transactions on Graphics*, Vol. 27, 2008, pp. 72:1-72:9.
6. K. M. He, J. Sun, and X. O. Tang, "Single image haze removal using dark channel prior," *IEEE Transactions on Pattern Analysis and Machine Intelligence*, Vol. 33, 2011, pp. 2341-2353.
7. S. Wei and H. Long, "A new fast single-image defog algorithm," in *Proceedings of IEEE 3rd International Conference on Intelligent System Design and Engineering Applications*, 2013, pp. 116-119.
8. J. P. Tarel and N. Hautiere, "Fast visibility restoration from a single color or gray level image," in *Proceedings of IEEE 12th International Conference on Computer Vision*, 2009, pp. 2201-2208.

9. W. Middleton, *Vision Through the Atmosphere*, University of Toronto Press, Toronto, Canada, 1952.
10. N. Hautiere, J. P. Tarel, J. Lavenant, and D. Aubert, "Automatic fog detection and estimation of visibility distance through use of an onboard camera," *Machine Vision and Applications*, Vol. 17, 2006, pp. 8-20.
11. International lighting vocabulary, 17.4, 1987.
12. M. D. Grossberg and S. K. Nayar, "Modeling the space of camera response functions," *IEEE Transactions on Pattern Analysis and Machine Intelligence*, Vol. 26, 2004, pp. 1272-1282.
13. K. Q. Huang, Q. Wang, and Z. Y. Wu, "Natural color image enhancement and evaluation algorithm based on human visual system," *Computer Vision and Image Understanding*, Vol. 103, 2006, pp. 52-63
14. S. Hasler and S. Susstrunk, "Measuring colorfulness in natural images," in *Proceedings of SPIE – The International Society for Optical Engineering*, Vol. 5007, 2003, pp. 87-95.
15. S. Yendrikhovskij, F. Blommaert, and H. D. Ridder, "Perceptual optimal color reproduction," in *Proceedings of the SPIE – The International Society for Optical Engineering*, Vol. 3299, 1998, pp. 274-281.
16. J. P. Tarel, N. Hautiere, A. Cord, and D. Gruyer, "Improved visibility of road scene images under heterogeneous fog," in *Proceedings of IEEE Intelligent Vehicle Symposium*, 2010, pp. 478-485.
17. J. H. Shan, "Lane mark recognition based on gray histogram," in *Proceedings of Conference on Cognitive Computing*, 2010, pp. 258-261 (in Chinese).
18. Z. X. Cai and M. Q. Gu, "Traffic sign recognition algorithm based on shape signature and dual tree-complex wavelet transform," *Journal of Central South University*, Vol. 20, 2013, pp. 433-439.

Fan Guo (郭璠) received the B.S. degree in Computer Science and Technology in 2005 and the M.S. and Ph.D. degrees in Computer Application Technology in 2008 and 2012, respectively, all from the Central South University (CSU), Changsha, China. Currently, she is a Postdoctoral Fellow and Lecturer with the School of Information Science and Engineering, CSU. Her main research interests include image processing, pattern recognition, and virtual reality.

Hui Peng (彭辉) received the B.Eng. and M.Eng. degrees in Control Engineering from Central South University (CSU), Changsha, China, in 1983 and 1986, respectively, and the Ph.D. degree in Statistical Science from the Graduate University for Advanced Studies, Hayama, Japan, in 2003. He is currently a Professor with the School of Information Science and Engineer-

ing, CSU. His research interests include nonlinear system modeling, statistical modeling, system identification, parameter optimization, signal processing, predictive control, robust control, and process control.

Jin Tang (唐琎) received the B.S. and M.S. degrees from Peking University, Beijing, China, in 1987 and 1990, respectively, and the Ph.D. degree in pattern recognition and intelligence system from Central South University (CSU), Hunan, China, in 2002. He is currently a Professor with the School of Information Science and Engineering, CSU, Changsha, China. His current research interests include image processing, pattern recognition, and computer vision.